


PAPER

[View Article Online](#)
[View Journal](#) | [View Issue](#)Cite this: *RSC Chem. Biol.*, 2022,
3, 1251A multicomponent reaction platform towards
multimodal near-infrared BODIPY dyes for STED
and fluorescence lifetime imaging†Antonio Fernandez, *^{ab} Nicola Kielland, ^{ac} Ashraff Makda, ^d Neil O. Carragher, ^d
M. Carmen González-García, ^e Laura Espinar-Barranco, ^e Juan A. González-Vera, ^e
Angel Orte, ^e Rodolfo Lavilla ^c and Marc Vendrell *^aReceived 18th July 2022,
Accepted 25th August 2022

DOI: 10.1039/d2cb00168c

rsc.li/rsc-chembio

We report a platform combining multicomponent reaction synthesis and automated cell-based screening to develop biocompatible NIR-BODIPY fluorophores. From a library of over 60 fluorophores, we optimised compound **NIRBD-62c** as a multimodal probe with suitable properties for STED super-resolution and fluorescence lifetime imaging. Furthermore, we employed **NIRBD-62c** for imaging trafficking inside cells and to examine how pharmacological inhibitors can alter the vesicular traffic between intracellular compartments and the plasma membrane.

Introduction

Intracellular trafficking involves the movement of biomolecules from synthetic compartments to locations where they can be released to the extracellular space.^{1–4} Cellular trafficking is heavily compartmentalized within a dynamic endomembrane network of subcellular organelles. The main vesicular organelles found in eukaryotic cells are lysosomes, the endoplasmic reticulum (ER) and the Golgi apparatus. The exchange of cargoes, membrane components and solutes between these organelles is a rapid process with an essential role in cellular homeostasis;^{5,6} therefore, disruptions in intracellular trafficking can lead to dysfunctional organelles and subsequent pathological disorders.^{7,8} As a result, chemical tools for real-time monitoring of vesicular transport inside live cells are crucial to understand their pathophysiology and to identify disease-specific signatures.^{9–12}

Recent advances in optical imaging have opened new opportunities for the design of chemical tools to monitor

intracellular trafficking.^{13–19} Among these, fluorescent probes are powerful tools for both sensing and optical imaging because of their high sensitivity, specificity and versatility.^{20–24} In addition, technical developments during the last decade have enabled the visualization of physiological processes with enhanced subcellular resolution.^{25–27} Different super-resolution microscopy modalities have been designed to overcome the conventional diffraction limit, with STimulated Emission Depletion (STED) being one of the most widespread techniques.^{28–30} Briefly, in STED a diffraction-limit region is excited at one wavelength while a super-imposed, high-power, red laser beam is projected to deplete most of the lateral emission and leave only a central focal spot with diameter under the diffraction limit.³¹ Using this approach, STED microscopy can provide fluorescence images with spatial resolution under 50 nm and temporal resolution in the range of milliseconds, offering a means to image the dynamics of intracellular functions in live cells.³²

Near-infrared (NIR) fluorophores are excellent tools for tracking biological processes inside cells in a non-invasive manner.^{33–39} In addition to minimizing the impact of tissue background fluorescence and maximizing photon penetration, STED depletion is more efficient in fluorophores excited by red and NIR light sources; however, the number of synthetic NIR fluorophores for super-resolution imaging of subcellular organelles remains limited.^{40–42} Therefore, the development of organelle-targeted responsive NIR fluorophores is an important step in the design of new approaches to visualize dynamic processes associated with intracellular trafficking.

Among the different organic fluorescent structures, we focused this work on the 4,4-difluoro-4-bora-3a,4a-diaza-s-indacene (BODIPY) scaffold.^{43–45} BODIPY is a widely employed

^a Centre for Inflammation Research, The University of Edinburgh, Edinburgh, UK.
E-mail: marc.vendrell@ed.ac.uk

^b Dpt Organic Chemistry, Faculty of Chemistry, University of Murcia, Spain.
E-mail: qjfvargas@ugr.es

^c Laboratory of Medicinal Chemistry, Faculty of Pharmacy and Institute of Biomedicine (IBUB), University of Barcelona, Spain

^d Institute of Genetics and Cancer, The University of Edinburgh, Edinburgh, UK

^e Nanoscopy-UGR Laboratory, Facultad de Farmacia, Universidad de Granada, Granada, Spain

† Electronic supplementary information (ESI) available: Chemical synthesis and characterization, protocols, figures and movies. See DOI: <https://doi.org/10.1039/d2cb00168c>

fluorophore in optical imaging because of its excellent photo-physical properties and cell permeability, which favours rapid accessibility to the endomembrane network of intracellular compartments. Recently, our group has demonstrated the suitability of BODIPY-based fluorophores for imaging membrane-associated events (*e.g.*, apoptosis) and receptor-mediated endocytic transport.^{15,20,46,47} Furthermore, we have demonstrated that the BODIPY core can be chemically diversified using multicomponent reactions to produce libraries of activatable fluorophores.⁴⁸ In view of this, we envisioned that synthetic methodologies based on multicomponent reactions would accelerate the synthesis and optimization of new probes for super-resolution microscopy in the NIR range. Herein, we present the chemical synthesis of a new collection of NIR BODIPY probes and their validation for imaging cellular trafficking using STED and fluorescence lifetime imaging.

Results and discussion

Design and synthesis of a library of pH-activatable NIR BODIPYs

Discovered by Lieke in 1859,⁴⁹ isonitriles, which formally feature divalent carbon atoms, have become a pivotal functional group for multicomponent reaction chemistry and are

broadly used in the modern production of diversity-oriented libraries of peptides and small molecules.^{50–53} Isonitrile-based multi-component reactions constitute a step forward in fluorophore derivatization;⁵⁴ however, to the best of our knowledge, they have not been previously reported for the diversification of NIR BODIPY dyes. Based on our experience with pH-activatable fluorophores for monitoring vesicle trafficking, we designed a library of NIR BODIPY fluorophores with the formamide **2** (Fig. 1) as the main precursor, enabling *in situ* generation of isonitriles and subsequent derivatization into pH-sensitive fluorophores *via* multicomponent reaction chemistry. We synthesized the NIR-emitting formamide **2** by performing a double Knoevenagel condensation between *p*-anisaldehyde and the green-fluorescent BODIPY formamide **1** (Fig. 1). As expected, the condensation reaction took place between the α -methyl groups in the positions 3 and 5 of the BODIPY scaffold,^{55,56} yielding the double adduct in good yields (around 60%). The π -extended BODIPY formamide was dehydrated with POCl₃ and DIPEA to generate the isonitrile **3** in quantitative yields, being the starting material to generate a collection of NIR BODIPY (NIRBD) dyes.

To study the versatility and application of the isonitrile **3** for the combinatorial generation of novel NIR fluorophores, we subjected the isonitrile **3** to the Ugi three-component reaction using formic acid, formaldehyde as a non-stereogenic carbonyl

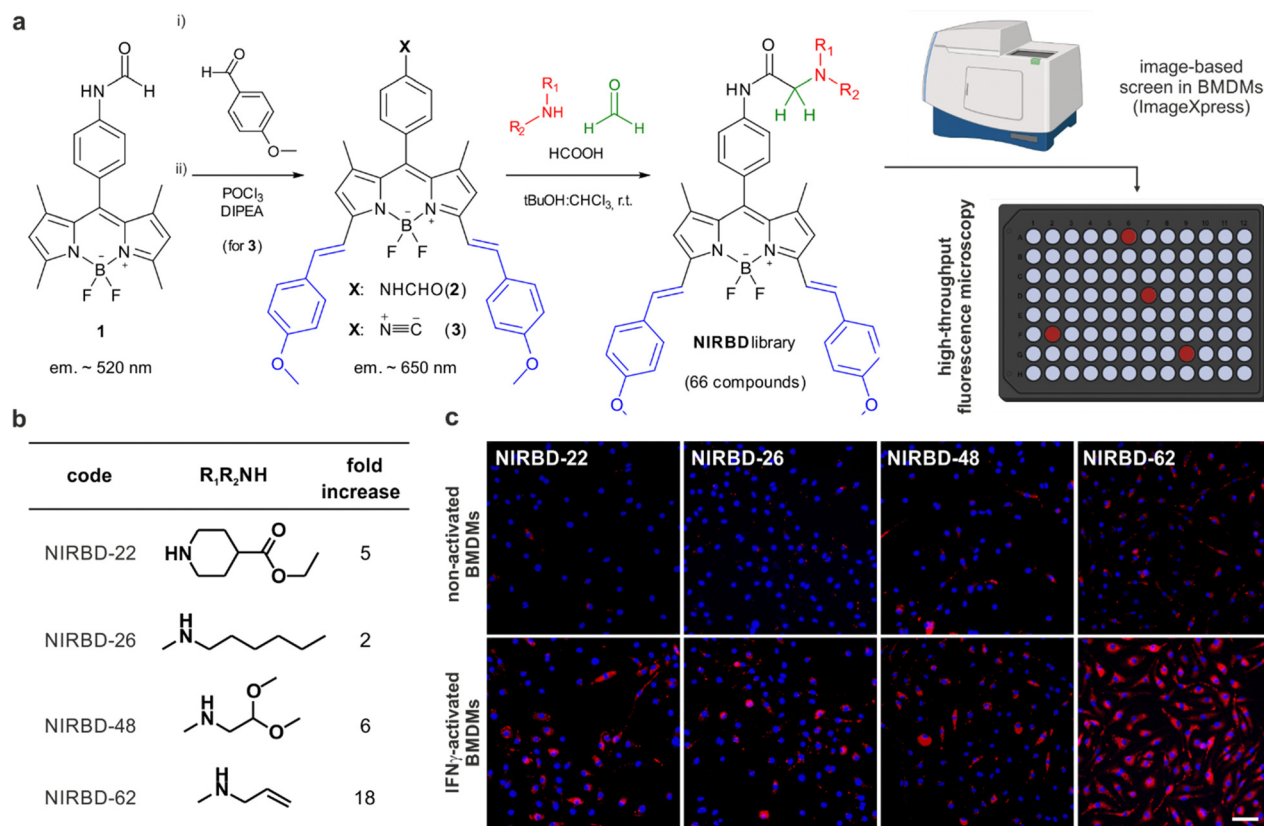


Fig. 1 Synthesis and screening of the NIRBD library. (a) Chemical synthesis of NIRBD fluorophores and high-throughput screening in BMDMs. (b) Chemical structures and fluorescence fold increase in acid pH vs. neutral pH of selected NIRBD compounds. (c) Representative microscopy images of live BMDMs (20×) after incubation with Hoechst (blue) and NIRBD dyes (red). Scale bar: 50 μm.



input and a range of over 60 structurally-diverse amines to generate the corresponding α -aminoamides (Fig. 1). Because α -aminoamides can affect the push-pull dipole in a pH-dependent manner, we envisaged that they would be suitable chemical groups to generate profluorophores that would turn-on in the acidic environments found in intracellular vesicles (e.g., lysosomes, endosomes, phagosomes). Using this approach, we synthesized a library of 66 new NIR BODIPYs (Table S1, ESI† for detailed structures and characterization). Next, we performed automated high content image-based fluorescence screening in non-activated and phagocytic bone marrow-derived macrophages (BMDMs) to identify NIR fluorophores that would preferentially emit in phagocytic cells with enhanced trafficking activity. We ran a fluorescence-based screening where we cultured BMDMs in the absence or presence of interferon (IFN)- γ ,⁵⁷ followed by incubation with the NIRBD dyes. We acquired fluorescence microscopy images, using the ImageXpress high content screening platform, in both non-activated and IFN γ -activated cells and identified NIRBD dyes (**NIRBD-22,26,48,62**) with brighter emission in phagocytic cells (Fig. 1). Further *in vitro* assays at different pH values confirmed that all shortlisted NIRBD compounds were brighter in acidic environments when compared to the pH-insensitive isonitrile **3** (Fig. S1, ESI†).

After image analysis, we concluded that the *N*-allylmethylamine derivative **NIRBD-62** showed the highest fold fluorescence increase between non-activated and activated BMDMs (Fig. 1), which was also replicated *in vitro* (Fig. S1, ESI†). Therefore, we selected this amine for further optimization of the NIRBD scaffold to generate new STED fluorophores for imaging intracellular trafficking in live cells.

Optimization of water-soluble NIRBD fluorophores

One of the most common limitations of NIR fluorophores is their reduced compatibility in aqueous media, which can lead to large aggregates and imaging artifacts. We analyzed the water solubility properties of **NIRBD-62** and observed significant aggregation in phosphate buffer saline (PBS, Fig. 2), which hampered its utility in live-cell imaging experiments. NIR fluorophores, including BODIPYs and cyanines, can be readily modified with water-solubilizing groups (e.g., sulfonates);⁵⁸ however, the inclusion of negative charges within the NIRBD core might impair its affinity for the lipophilic domains of the endomembrane network. Therefore, we decided to optimize the chemical structure of **NIRBD-62** by fine-tuning the styryl fragments of the BODIPY core (Fig. 2).

Based on predicted log *P* values, we selected two commercially available aldehydes that could decrease the lipophilicity of NIR BODIPYs to prepare more water-soluble analogues of **NIRBD-62** (**NIRBD-62a** and **NIRBD-62b**, Fig. 2 and Fig. S2, ESI†). We synthesized **NIRBD-62a** and **NIRBD-62b** following the same strategy outlined in Fig. 1 (for full synthetic and characterization details, see ESI†). First, we performed Knoevenagel-like condensations using the two new aldehydes and the BODIPY formamide **1**. The two NIR-BODIPY formamides were converted to the respective isonitriles and derivatized with *N*-allylmethylamine in a

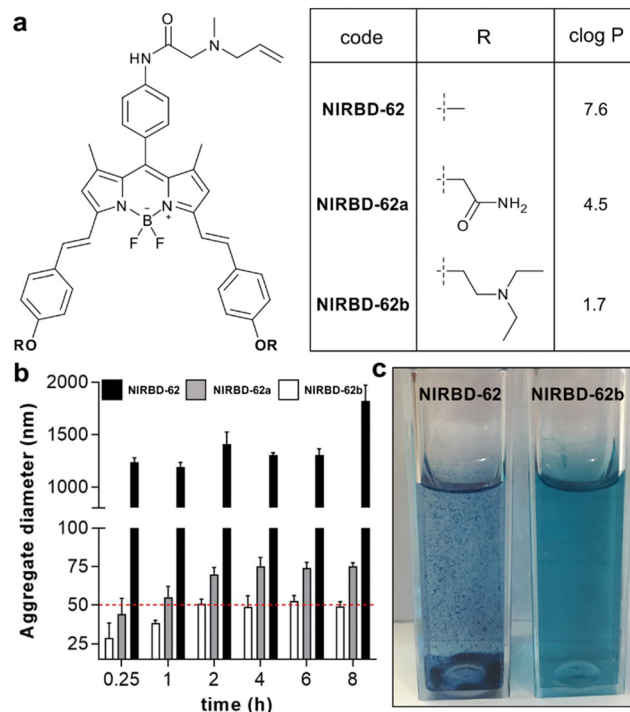


Fig. 2 Optimization of the water solubility profile of NIR-BODIPY fluorophores. (a) Chemical structures of the styryl-functionalized NIRBD dyes and predicted clog *P* values for each derivative (chemical synthesis and full characterization in ESI†). (b) Time-course analysis of aggregate formation of **NIRBD-62** analogues in aqueous media (100 μ M in PBS) determined by dynamic light scattering at 25 $^{\circ}$ C for 8 h. Relative threshold for solubility at aggregates under 50 nm diameter (red). Values represented as means \pm SD ($n = 3$). For compound **NIRBD-62b**, no detectable aggregates were found at lower concentrations (1–5 μ M in PBS). (c) Representative photographs of cuvettes containing solutions of compounds **NIRBD-62** and **NIRBD-62b** in aqueous media (100 μ M in PBS).

multicomponent approach with formaldehyde and formic acid to render the final products in moderate overall yields (around 20%) and high purities (>95%). Next, we compared the water solubility of the original compound **NIRBD-62** and the new analogues by measuring the formation of aggregates over time using dynamic light scattering. We observed that both compounds **NIRBD-62a** and **NIRBD-62b** showed a markedly reduced tendency to form aggregates in PBS when compared to **NIRBD-62** (Fig. 2), with **NIRBD-62b** being the most water-soluble analogue. Furthermore, the qualitative analysis of 100 μ M NIRBD solutions in PBS showed much reduced aggregation in the case of **NIRBD-62b**, even after the compound had been in aqueous solution for several hours, which features its good water solubility. Finally, we confirmed that the modification of the styryl group in **NIRBD-62b** did not alter the ability to label intracellular compartments in phagocytic cells (Fig. S3 and S4, ESI†).

STED and fluorescence lifetime imaging using NIR-BODIPYs

STED microscopy is an excellent technique for high-resolution structural imaging⁵⁹ but, unlike ratiometric imaging or fluorescence lifetime imaging (FLIM), it cannot provide quantitative



information. FLIM uses the luminescence decay rate and determines the corresponding luminescence lifetime (τ) of a given fluorophore as the parameter of interest. Unlike intensity-based measurements, FLIM is concentration-independent and therefore avoids the need for normalization factors.^{59,60} Therefore, the recent integration of FLIM with super-resolution microscopy (e.g., STED-FLIM),⁶¹ combines the advantages of both modalities. To assess the usefulness of the NIRBD dyes in advanced STED-FLIM experiments, we first determined the τ values of compound **NIRBD-62b** in different solvents and observed very low τ values (< 2 ns), which hampered its utility for FLIM experiments. To address this point, we decided to include a methoxy group in the meso aryl ring of the NIR BODIPY scaffold that would minimize non-radiative decay *via* restriction of rotational processes.⁶² The resulting **NIRBD-62c** (Fig. 3 and ESI†, for chemical synthesis and full characterization) displayed very high fluorescence quantum yields (from 25% in

water to $> 95\%$ in 1,4-dioxane, Fig. S5, ESI†) and consistently high τ values around 4 ns in different environments, which would be readily distinguishable from the cellular background (e.g., NADPH, flavonoids) in FLIM experiments (Fig. 3). Furthermore, we acquired the fluorescence spectra of **NIRBD-62c** in multiple solvents (Fig. S6, ESI†). Notably, in addition to showing polarity-dependent emission maxima around 645 ± 10 nm, the compound **NIRBD-62c** also exhibited secondary, high-energy maxima at 590 nm and additional longer emission bands ~ 720 nm (Fig. S6, ESI†). This unique multiband emission profile makes **NIRBD-62c** an optimal NIR fluorophore for ratiometric fluorescence imaging.

Given the photophysical features of **NIRBD-62c** as a bright and water-compatible NIR-emitting fluorophore, we tested its capabilities for super-resolution STED and STED-FLIM microscopy. An important feature in organic fluorophores for STED microscopy is their photostability upon excitation with the high-power depletion laser. First, we examined **NIRBD-62c** and observed bright and consistent fluorescence emission > 650 nm during the $60 \mu\text{s}$ per pixel irradiation regime typically used for STED microscopy. Next, we compared the resolution of fluorescence microscopy images of live mouse osteoblasts (MC3T3-E1) obtained sequentially under regular confocal microscopy and STED microscopy. As shown in Fig. 3, we observed a significant improvement in image resolution for the latter, which highlights the compatibility of compound **NIRBD-62c** for super-resolution imaging. Notably, STED images exhibited well-defined subcellular vesicles containing the fluorophore in the perinuclear region and close to the cellular membrane (Fig. 3).

Next, we decided to exploit the multiband emission profile of **NIRBD-62c** to acquire ratiometric microscopy images in combination with FLIM in live osteoblasts. To perform these multiparametric imaging experiments, we used a dual-color FLIM set-up (Fig. 4), which consisted of a pulsed 635 nm excitation laser and two single-photon detection channels with bandpass filters of 685/70 (I_{685}) and 750/40 (I_{750}), allowing the reconstruction of both fluorescence lifetime and ratiometric images (I_{685}/I_{750}). The ratiometric images obtained from the polarity-sensitive fluorescence band > 650 nm (close the **NIRBD-62c** maxima) and the long-emission band > 700 nm (Fig. S6, ESI†) highlighted the sensitivity of compound **NIRBD-62c** to different subcellular microenvironments, with the brightest regions being around perinuclear compartments and slightly weaker staining detected on the cell membranes. Notably, such differences were detected under FLIM too. In this case, **NIRBD-62c** showed τ values around 4.2 ns (28 regions of interest, ROI) in the perinuclear regions whereas slightly longer τ values 4.4 ns (40 ROIs) were found in the cytoplasmic membrane (Fig. 4 and Movies S1 and S2, ESI†). Altogether, these observations highlight that compound **NIRBD-62c** can distribute across different compartments of the endomembrane network, and that its localization can be monitored by ratiometric fluorescence imaging as well as FLIM.

In order to examine the underlying mechanisms behind the environmental sensitivity of compound **NIRBD-62c**, we applied

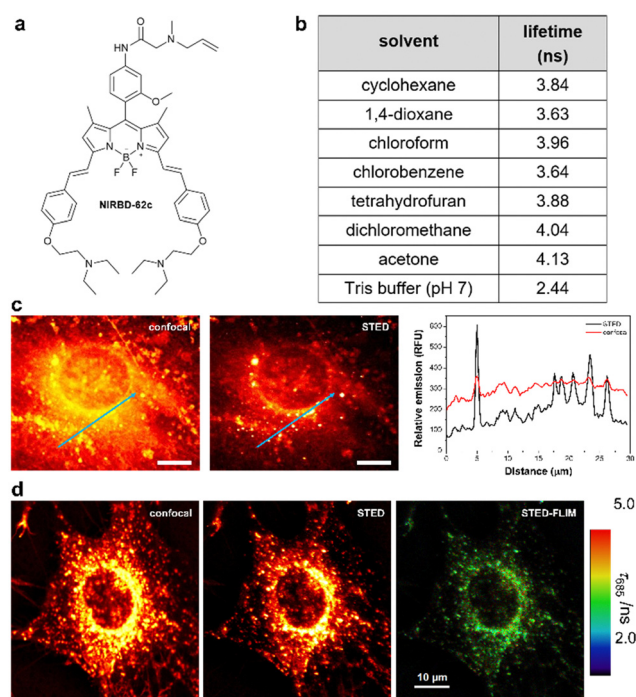


Fig. 3 **NIRBD-62c** is a suitable fluorophore for multimodal STED and fluorescence lifetime imaging. (a) Chemical structure of the fluorophore **NIRBD-62c** (chemical synthesis and full characterization in ESI†). (b) Fluorescence lifetimes (τ) of compound **NIRBD-62c** in different solvents determined by time-resolved fluorimetry in single photon timing mode, using a 635 nm excitation laser. Values obtained from global fits of 3 measurements at different emission wavelengths, showing associated errors in the fittings lower than 0.03 ns in all cases. (c) Representative fluorescence microscopy images and associated intensity plot profiles of MC3T3-E1 osteoblasts upon incubation with **NIRBD-62c** (100 nM) under conventional fluorescence confocal microscopy and STED microscopy. Both images were simultaneously acquired using one pulse of 640 nm excitation laser (for confocal) and three pulses of excitation + depletion laser (for STED). Emission was collected using a 685/70 bandpass filter. (d) Representative STED-FLIM pseudocolored image, using the same configuration as in (c) and after performing a pixelwise tail-fit of the fluorescence decay to estimate τ values.



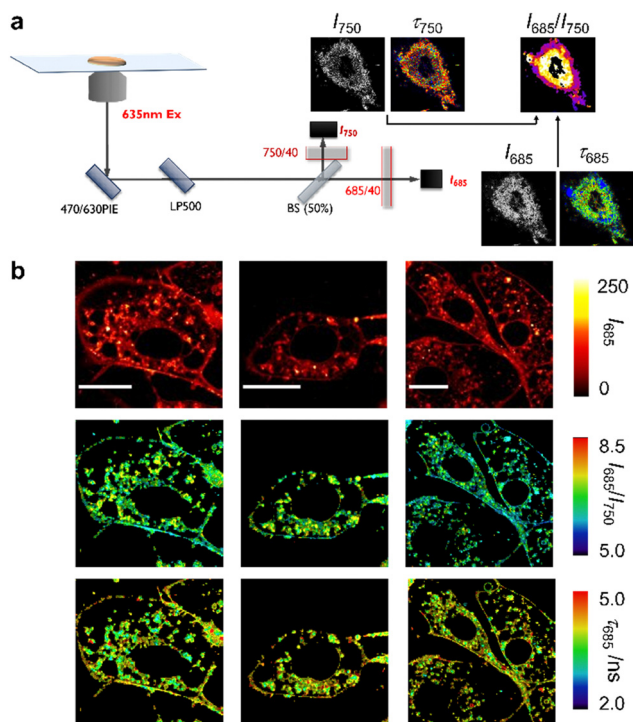


Fig. 4 Multiparametric fluorescence microscope images of live mouse osteoblasts upon incubation with the compound **NIRBD-62c**. (a) Schematic illustration of the multiparametric fluorescence microscopy set-up. (b) Representative pseudocolored images from 3 different groups of MC3T3-E1 cells using the fluorescence intensity in the 685 nm channel (top row), the fluorescence ratiometric I_{685}/I_{750} measurements (middle row) and the fluorescence lifetime in the 685 nm channel (bottom row). The cells were incubated with 100 nM of compound **NIRBD-62c** before imaging. Scale bar: 20 μ m.

the methodology developed by Catalán to study its solvatochromic features.⁶³ This methodology allows to correlate photo-physical properties of a given fluorophore to the main features of different organic solvents, such as polarity, polarizability, acidity, and basicity. Specifically, we examined the absorption and emission maxima wavelengths of **NIRBD-62c** in multiple organic solvents (Fig. S6, ESI†) and found that the main solvent property that affected both absorption and emission maxima was polarizability (Fig. S7, ESI†). This behavior is likely due to the large size of **NIRBD-62c**, which leads to the dispersion interactions between the electron clouds of the fluorophore and the solvents defining ground and excited-state stabilization upon solvation. In addition to polarizability, we also observed that the acidity and basicity of the media also contributed to the excited-state stabilization. This is expected for pH-sensitive fluorophores like the NIRBD compounds and suggests that hydrogen bonding interactions are involved in the relaxation processes. Moreover, we analyzed the I_{685}/I_{750} ratios of compound **NIRBD-62c** vs. the polarity and polarizability of solvents, and observed a direct correlation between the intensity ratios and both parameters, with the I_{685}/I_{750} ratio increasing with solvent polarity and decreasing with solvent polarizability. These results confirm that the I_{685}/I_{750} ratios acquired in

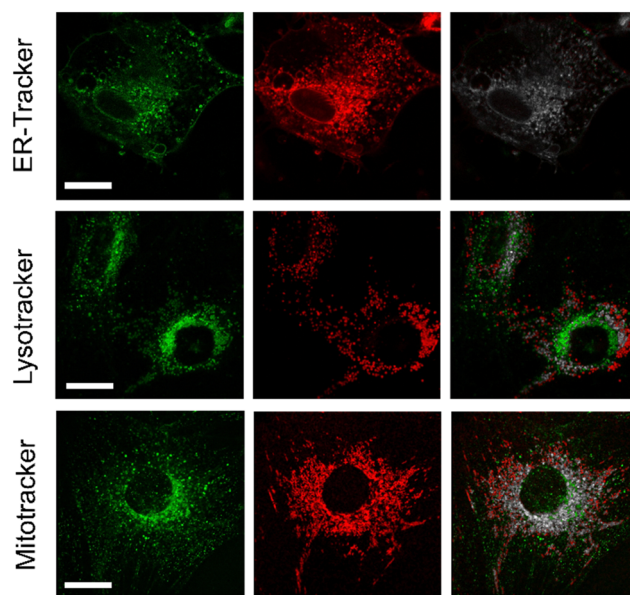


Fig. 5 Co-localization fluorescence microscopy of compound **NIRBD-62c** with organelle fluorescent trackers. Representative confocal microscopy images from live-cell osteoblasts upon incubation with compound **NIRBD-62c** (green) and commercially available organelle trackers (red). Co-localization areas are highlighted in grey in the merged fluorescence images. Scale bar: 20 μ m.

microscopy experiments can be considered as direct reporters of the fluorophore's microenvironment.

Next, we decided to examine the distribution of compound **NIRBD-62c** in different subcellular organelles. For these experiments, we performed co-localization experiments where we incubated cells with both **NIRBD-62c** and different commercially available trackers (*i.e.*, ER-Tracker, LysoTracker and Mitotracker). As shown in Fig. 5, most of the intracellular staining of compound **NIRBD-62c** was found in vesicular structures around the ER, with little accumulation in mitochondria or lysosomes. This result, together with the partial localization of the fluorophore observed in the cellular membrane (Fig. 4), suggest that compound **NIRBD-62c** holds potential as a fluorophore to monitor intracellular trafficking processes from the ER to the plasma membrane and the extracellular space.

Finally, we decided to study whether the fluorescence read-outs of compound **NIRBD-62c** could be used to monitor alterations in intracellular trafficking. For these experiments, we used some reported pharmacological inhibitors; specifically: (1) dynasore, a non-competitive dynamin inhibitor that blocks endocytic pathways⁶⁴ and (2) brefeldin A (BFA),⁶⁵ an antiviral drug that inhibits protein transport from the ER to the Golgi complex.

First, we observed that the fluorescence emission of compound **NIRBD-62c** was drastically reduced (*i.e.*, >5-fold decrease) upon treatment with dynasore when compared to untreated or BFA-treated cells (Fig. S8, ESI†). Moreover, dynasore-treated cells exhibited the compound mostly trapped in O-shape invaginations near the plasma membrane (Fig. 6), consistent with the effect of dynasore as a dynamin inhibitor,



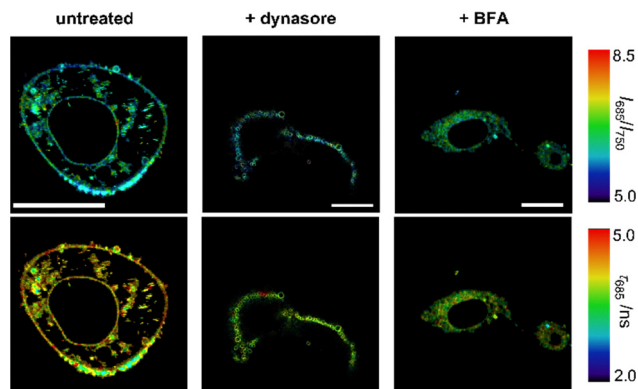


Fig. 6 Multiparametric fluorescence microscopy of **NIRBD-62c** in cells upon treatment with different pharmacological inhibitors. Representative pseudocolored images from 3 different groups of cells (all incubated with **NIRBD-62c**, 100 nM) that were untreated, treated with dynasore (80 μ M) or BFA (5 μ M). Microscopy images display ratiometric measurements (top row) as well as fluorescence lifetime measurements (bottom row). For ratiometric images, pseudocolors indicate the fluorescence intensity ratios of compound **NIRBD-62c** at 685 nm vs. 750 nm. For FLIM images, pseudocolors indicate the variations in the fluorescence lifetimes (emission: 685 nm) of **NIRBD-62c** in different subcellular regions. Scale bar: 20 μ m.

which leads to clathrin-coated vesicles trapped in the plasma membrane.⁶⁶ This observation suggested that endocytosis plays an important role in the internalization of **NIRBD-62c**. To further analyze this point, we incubated cells at 4 °C to minimize endocytic trafficking. In these experiments, we found bright staining in the ER-Golgi system but a drastically reduced number of intracellular vesicles (Fig. S9, ESI[†]), suggesting that the uptake of **NIRBD-62c** can proceed through both endocytic transport and passive diffusion. On the other hand, the treatment with BFA led to minor differences in fluorescence intensity (Fig. S8, ESI[†]) but drastic variations in the localization of compound **NIRBD-62c**. Specifically, the labelling of the plasma membrane was reduced in BFA-treated cells and led to the accumulation of the fluorophore in the perinuclear region. This observation suggests that the blockade of the transport between the ER and Golgi apparatus is important for vesicular trafficking to the cell membrane and subsequent exocytosis. Notably, in addition to the differences in intracellular localization, we corroborated this observation by FLIM. As shown in Fig. 6 and Fig. S8 (ESI[†]), **NIRBD-62c** displayed longer τ values in untreated cells with brighter plasma membrane localization than in BFA-treated cells – with brighter accumulation in perinuclear compartments, such as the ER-, which is in line with the fluorescence lifetimes found for compound **NIRBD-62c** in different subcellular regions.

Conclusions

In summary, we have designed a platform for the synthesis and high-throughput screening of new NIR-BODIPY fluorophores that enable live-cell imaging of intracellular trafficking. Herein we report one of the first examples of isonitrile-functionalized

NIR scaffolds and their derivatization by multicomponent reaction chemistry to generate collections of new fluorophores.

We envision that the adaptation of this synthetic strategy to other fluorophores will accelerate the design of NIR probes. From an initial library of 60+ NIR fluorophores, we have optimized **NIRBD-62c** as a single multimodal probe with good water solubility and suitable properties for ratiometric confocal imaging, STED super-resolution imaging and FLIM. We have applied multiparametric fluorescence imaging and pharmacological inhibitors to confirm that **NIRBD-62c** predominantly locates in the ER of live cells and can monitor intracellular traffic to the plasma membrane. **NIRBD-62c** and future derivatives hold potential as novel non-invasive imaging tools to study how molecules translocate across subcellular compartments.

Author contributions

Conceptualization: A. F., N. K., R. L. and M. V.; funding acquisition: A. F., J. A. G. V., A. O., R. L., M. V.; investigation: A. F., N. K., A. M., M. C. G. G., L. E. B., J. A. G. V. and M. V.; resources: N. O. C.; supervision: N. O. C., J. A. G. V., A. O., R. L., M. V.; writing – original draft: A. F. and M. V.; writing – review & editing: A. F., N. O. C., A. O., R. L. and M. V.

Conflicts of interest

The authors have no conflicts to declare.

Acknowledgements

A. F. acknowledges the support of Fundación Séneca for the Saavedra Fajardo Grant (21124/SF/19). A. O. and J. A. G. V. acknowledge the grant PID2020-114256RB-I00 from MCIN/AEI/10.13039/501100011033. R. L. acknowledges funding from the Ministry of Science and Innovation-Spain (PID2019-107991RB-I00). M. V. acknowledges funding from an ERC Consolidator Grant (771443) and the Royal Society (RG160289).

Notes and references

- 1 J. L. Stow and R. Z. Murray, Intracellular trafficking and secretion of inflammatory cytokines, *Cytokine Growth Factor Rev.*, 2013, **24**, 227–239.
- 2 M. Kalim, J. Chen, S. Wang, C. Lin, S. Ullah, K. Liang, Q. Ding, S. Chen and J. Zhan, Intracellular trafficking of new anticancer therapeutics: antibody-drug conjugates, *Drug Des., Devel. Ther.*, 2017, **11**, 2265–2276.
- 3 H. M. York, J. Coyle and S. Arumugam, To be more precise: the role of intracellular trafficking in development and pattern formation, *Biochem. Soc. Trans.*, 2020, **48**, 2051–2066.
- 4 K. Morl and A. G. Beck-Sicking, Intracellular trafficking of neuropeptide Y receptors, *Prog. Mol. Biol. Transl. Sci.*, 2015, **132**, 73–96.



- 5 K. Mishev, W. Dejonghe and E. Russinova, Small molecules for dissecting endomembrane trafficking: a cross-systems view, *Chem. Biol.*, 2013, **20**, 475–486.
- 6 F. Arenas, C. Garcia-Ruiz and J. C. Fernandez-Checa, Intracellular cholesterol trafficking and impact in neurodegeneration, *Front. Mol. Neurosci.*, 2017, **10**, 382.
- 7 H. Zhu, J. Fan, J. Du and X. Peng, Fluorescent probes for sensing and imaging within specific cellular organelles, *Acc. Chem. Res.*, 2016, **49**, 2115–2126.
- 8 S. Shanmughapriya, D. Langford and K. Natarajaseenivasan, Inter and intracellular mitochondrial trafficking in health and disease, *Ageing Res. Rev.*, 2020, **62**, 101128.
- 9 R. N. Germain, E. A. Robey and M. D. Cahalan, A decade of imaging cellular motility and interaction dynamics in the immune system, *Science*, 2012, **336**, 1676–1681.
- 10 X. Wang, Z. Zeng, J. H. Jiang, Y. T. Chang and L. Yuan, Discerning the chemistry in individual organelles with small-molecule fluorescent probes, *Angew. Chem., Int. Ed.*, 2016, **55**, 13658–13699.
- 11 K. Zhanghao, W. Liu, M. Li, Z. Wu, X. Wang, X. Chen, C. Shan, H. Wang, X. Chen, Q. Dai, P. Xi and D. Jin, High-dimensional super-resolution imaging reveals heterogeneity and dynamics of subcellular lipid membranes, *Nat. Commun.*, 2020, **11**, 5890.
- 12 D. I. Danylchuk, P. H. Jouard and A. S. Klymchenko, Targeted solvatochromic fluorescent probes for imaging lipid order in organelles under oxidative and mechanical stress, *J. Am. Chem. Soc.*, 2021, **143**, 912–924.
- 13 A. J. Wilson, D. Devasia and P. K. Jain, Nanoscale optical imaging in chemistry, *Chem. Soc. Rev.*, 2020, **49**, 6087–6112.
- 14 Z. M. Cheng, E. Kuru, A. Sachdeva and M. Vendrell, Fluorescent amino acids as versatile building blocks for chemical biology, *Nat. Rev. Chem.*, 2020, **4**, 275–290.
- 15 R. Subiros-Funosas, L. Mendive-Tapia, J. Sot, J. D. Pound, N. Barth, Y. Varela, F. M. Goni, M. Paterson, C. D. Gregory, F. Albericio, I. Dransfield, R. Lavilla and M. Vendrell, A Trp-BODIPY cyclic peptide for fluorescence labelling of apoptotic bodies, *Chem. Commun.*, 2017, **53**, 945–948.
- 16 A. Fernandez, M. Vermeren, D. Humphries, R. Subiros-Funosas, N. Barth, L. Campana, A. MacKinnon, Y. Feng and M. Vendrell, Chemical modulation of in vivo macrophage function with subpopulation-specific fluorescent prodrug conjugates, *ACS Cent. Sci.*, 2017, **3**, 995–1005.
- 17 C. Zhao, A. Fernandez, N. Avlonitis, G. Vande Velde, M. Bradley, N. D. Read and M. Vendrell, Searching for the optimal fluorophore to label antimicrobial peptides, *ACS Comb. Sci.*, 2016, **18**, 689–696.
- 18 D. Cheng, W. Xu, X. Gong, L. Yuan and X. B. Zhang, Design strategy of fluorescent probes for live drug-induced acute liver injury imaging, *Acc. Chem. Res.*, 2021, **54**, 403–415.
- 19 T. B. Ren, Z. Y. Wang, Z. Xiang, P. Lu, H. H. Lai, L. Yuan, X. B. Zhang and W. Tan, A general strategy for development of activatable NIR-II fluorescent probes for in vivo high-contrast bioimaging, *Angew. Chem., Int. Ed.*, 2021, **60**, 800–805.
- 20 A. Fernandez, E. J. Thompson, J. W. Pollard, T. Kitamura and M. Vendrell, A fluorescent activatable AND-gate chemokine CCL2 enables in vivo detection of metastasis-associated macrophages, *Angew. Chem., Int. Ed.*, 2019, **58**, 16894–16898.
- 21 L. Mendive-Tapia, R. Subiros-Funosas, C. Zhao, F. Albericio, N. D. Read, R. Lavilla and M. Vendrell, Preparation of a Trp-BODIPY fluorogenic amino acid to label peptides for enhanced live-cell fluorescence imaging, *Nat. Protoc.*, 2017, **12**, 1588–1619.
- 22 S. J. Park, H. C. Yeo, N. Y. Kang, H. Kim, J. Lin, H. H. Ha, M. Vendrell, J. S. Lee, Y. Chandran, D. Y. Lee, S. W. Yun and Y. T. Chang, Mechanistic elements and critical factors of cellular reprogramming revealed by stepwise global gene expression analyses, *Stem Cell Res.*, 2014, **12**, 730–741.
- 23 L. Wu, J. Liu, X. Tian, R. R. Groleau, S. D. Bull, P. Li, B. Tang and T. D. James, Fluorescent probe for the imaging of superoxide and peroxynitrite during drug-induced liver injury, *Chem. Sci.*, 2021, **12**, 3921–3928.
- 24 X. Tian, L. C. Murfin, L. Wu, S. E. Lewis and T. D. James, Fluorescent small organic probes for biosensing, *Chem. Sci.*, 2021, **12**, 3406–3426.
- 25 S. Benson, A. Fernandez, N. D. Barth, F. de Moliner, M. H. Horrocks, C. S. Herrington, J. L. Abad, A. Delgado, L. Kelly, Z. Chang, Y. Feng, M. Nishiura, Y. Hori, K. Kikuchi and M. Vendrell, SCOTfluors: small, conjugatable, orthogonal, and tunable fluorophores for in vivo imaging of cell metabolism, *Angew. Chem., Int. Ed.*, 2019, **58**, 6911–6915.
- 26 D. Wu, H. C. Daly, M. Grossi, E. Conroy, B. Li, W. M. Gallagher, R. Elmes and D. F. O'Shea, RGD conjugated cell uptake off to on responsive NIR-AZA fluorophores: applications toward intraoperative fluorescence guided surgery, *Chem. Sci.*, 2019, **10**, 6944–6956.
- 27 M. Grossi, M. Morgunova, S. Cheung, D. Scholz, E. Conroy, M. Terrile, A. Panarella, J. C. Simpson, W. M. Gallagher and D. F. O'Shea, Lysosome triggered near-infrared fluorescence imaging of cellular trafficking processes in real time, *Nat. Commun.*, 2016, **7**, 10855.
- 28 G. Lukinavičius, K. Umezawa, N. Olivier, A. Honigsmann, G. Yang, T. Plass, V. Mueller, L. Reymond, I. R. Corrêa Jr, Z.-G. Luo, C. Schultz, E. A. Lemke, P. Heppenstall, C. Eggeling, S. Manley and K. Johnsson, A near-infrared fluorophore for live-cell super-resolution microscopy of cellular proteins, *Nat. Chem.*, 2013, **5**, 132–139.
- 29 M. Weber, T. A. Khan, L. J. Patalag, M. Bossi, M. Leutenegger, V. N. Belov and S. W. Hell, Photoactivatable fluorophore for stimulated emission depletion (STED) microscopy and bioconjugation technique for hydrophobic labels, *Chem. – Eur. J.*, 2021, **27**, 451–458.
- 30 V. Inavalli, M. O. Lenz, C. Butler, J. Angibaud, B. Compans, F. Levet, J. Tonnesen, O. Rossier, G. Giannone, O. Thoumine, E. Hosy, D. Choquet, J. B. Sibarita and U. V. Nagerl, A super-resolution platform for correlative live single-molecule imaging and STED microscopy, *Nat. Methods*, 2019, **16**, 1263–1268.
- 31 H. Blom and J. Widengren, Stimulated emission depletion microscopy, *Chem. Rev.*, 2017, **117**, 7377–7427.
- 32 E. Wegel, A. Göhler, B. C. Lagerholm, A. Wainman, S. Uphoff, R. Kaufmann and I. M. Dobbie, Imaging cellular



- structures in super-resolution with SIM, STED and Localisation Microscopy: A practical comparison, *Sci. Rep.*, 2016, **6**, 27290.
- 33 S. I. Reja, M. Minoshima, Y. Hori and K. Kikuchi, Near-infrared fluorescent probes: a next-generation tool for protein-labeling applications, *Chem. Sci.*, 2021, **12**, 3437–3447.
 - 34 R. J. Mellanby, J. I. Scott, I. Mair, A. Fernandez, L. Saul, J. Arlt, M. Moral and M. Vendrell, Tricarbocyanine N-triazoles: the scaffold-of-choice for long-term near-infrared imaging of immune cells in vivo, *Chem. Sci.*, 2018, **9**, 7261–7270.
 - 35 M. Grossi, M. Morgunova, S. Cheung, D. Scholz, E. Conroy, M. Terrile, A. Panarella, J. C. Simpson, W. M. Gallagher and D. F. O'Shea, Lysosome triggered near-infrared fluorescence imaging of cellular trafficking processes in real time, *Nat. Commun.*, 2016, **7**, 10855.
 - 36 L. Yuan, W. Lin, K. Zheng, L. He and W. Huang, Far-red to near infrared analyte-responsive fluorescent probes based on organic fluorophore platforms for fluorescence imaging, *Chem. Soc. Rev.*, 2013, **42**, 622–661.
 - 37 Y. Ge and D. F. O'Shea, Azadipyrromethenes: from traditional dye chemistry to leading edge applications, *Chem. Soc. Rev.*, 2016, **45**, 3846–3864.
 - 38 N. Toriumi, N. Asano, T. Ikeno, A. Muranaka, K. Hanaoka, Y. Urano and M. Uchiyama, Design of photostable, activatable near-infrared photoacoustic probes using tautomeric benzophthalocyanine as a platform, *Angew. Chem., Int. Ed.*, 2019, **58**, 7788–7791.
 - 39 R. J. Iwatate, M. Kamiya, K. Umezawa, H. Kashima, M. Nakadate, R. Kojima and Y. Urano, Silicon rhodamine-based near-infrared fluorescent probe for γ -glutamyltransferase, *Bioconjugate Chem.*, 2018, **29**, 241–244.
 - 40 E. Kozma and P. Kele, Fluorogenic probes for super-resolution microscopy, *Org. Biomol. Chem.*, 2019, **17**, 215–233.
 - 41 X. Zhang, L. Chen, Z. Huang, N. Ling and Y. Xiao, Cycloketal xanthene dyes: a new class of near-infrared fluorophores for super-resolution imaging of live cells, *Chem. – Eur. J.*, 2021, **27**, 3688–3693.
 - 42 J. B. Grimm, A. K. Muthusamy, Y. Liang, T. A. Brown, W. C. Lemon, R. Patel, R. Lu, J. J. Macklin, P. J. Keller, N. Ji and L. D. Lavis, A general method to fine-tune fluorophores for live-cell and in vivo imaging, *Nat. Methods*, 2017, **14**, 987–994.
 - 43 M. Virelli, W. Wang, R. Kuniyil, J. Wu, G. Zanoni, A. Fernandez, J. Scott, M. Vendrell and L. Ackermann, BODIPY-Labeled cyclobutanes by secondary C(sp³)-H arylations for live-cell imaging, *Chem. – Eur. J.*, 2019, **25**, 12712–12718.
 - 44 L. Mendive-Tapia, C. Zhao, A. R. Akram, S. Preciado, F. Albericio, M. Lee, A. Serrels, N. Kielland, N. D. Read, R. Lavilla and M. Vendrell, Spacer-free BODIPY fluorogens in antimicrobial peptides for direct imaging of fungal infection in human tissue, *Nat. Commun.*, 2016, **7**, 10940.
 - 45 T. Kowada, H. Maeda and K. Kikuchi, BODIPY-based probes for the fluorescence imaging of biomolecules in living cells, *Chem. Soc. Rev.*, 2015, **44**, 4953–4972.
 - 46 N. D. Barth, R. Subiros-Funosas, L. Mendive-Tapia, R. Duffin, M. A. Shields, J. A. Cartwright, S. T. Henriques, J. Sot, F. M. Goni, R. Lavilla, J. A. Marwick, S. Vermeren, A. G. Rossi, M. Egeblad, I. Dransfield and M. Vendrell, A fluorogenic cyclic peptide for imaging and quantification of drug-induced apoptosis, *Nat. Commun.*, 2020, **11**, 4027.
 - 47 N. Barth, L. Mendive-Tapia, R. Subiros-Funosas, O. Ghashghaie, R. Lavilla, L. Maiorino, X. Y. He, I. Dransfield, M. Egeblad and M. Vendrell, A bivalent activatable fluorescent probe for screening and intravital imaging of chemotherapy-induced cancer cell death, *Angew. Chem., Int. Ed.*, 2022, **61**, 202113020.
 - 48 A. Vázquez-Romero, N. Kielland, M. J. Arévalo, S. Preciado, R. J. Mellanby, Y. Feng, R. Lavilla and M. Vendrell, Multi-component reactions for de novo synthesis of BODIPY probes: in vivo imaging of phagocytic macrophages, *J. Am. Chem. Soc.*, 2013, **135**, 16018–16021.
 - 49 W. Lieke, Ueber das cyanallyl, *Justus Liebigs Ann. Chem.*, 1859, **112**, 316–321.
 - 50 A. Dömling, W. Wang and K. Wang, Chemistry and biology of multicomponent reaction, *Chem. Rev.*, 2012, **112**, 3083–3135.
 - 51 O. Ghashghaie, S. Caputo, M. Sintes, M. Reves, N. Kielland, C. Estarellas, F. J. Luque, A. Avino, R. Eritja, A. Serna-Gallego, J. A. Marrugal-Lorenzo, J. Pachon, J. Sanchez-Céspedes, R. Treadwell, F. de Moliner, M. Vendrell and R. Lavilla, Multiple multicomponent reactions: unexplored substrates, selective processes, and versatile chemotypes in biomedicine, *Chem. – Eur. J.*, 2018, **24**, 14513–14521.
 - 52 F. Yraola, R. Ventura, M. Vendrell, A. Colombo, J. C. Fernandez, N. Figuera, D. Fernandez-Forner, M. Royo, P. Fornis and F. Albericio, A re-evaluation of the use of Rink, BAL, and PAL resins and linkers, *QSAR Comb. Sci.*, 2004, **23**, 145–152.
 - 53 A. Dömling and I. Ugi, Multicomponent reactions with isocyanides, *Angew. Chem., Int. Ed.*, 2000, **39**, 3168–3210.
 - 54 O. N. Burchak, L. Mugherli, M. Ostuni, J. J. Lacapere and M. Y. Balakirev, Combinatorial discovery of fluorescent pharmacophores by multicomponent reactions in droplet arrays, *J. Am. Chem. Soc.*, 2011, **133**, 10058–10061.
 - 55 O. A. Bozdemir, R. Guliyev, O. Buyukcakil, S. Selcuk, S. Kolemen, G. Gulseren, T. Nalbantoglu, H. Boyaci and E. U. Akkaya, Selective manipulation of ICT and PET Processes in styryl-Bodipy derivatives: applications in molecular logic and fluorescence sensing of metal ions, *J. Am. Chem. Soc.*, 2010, **132**, 8029–8036.
 - 56 Z. Ekmekci, M. D. Yilmaz and E. U. Akkaya, A monostyryl-boradiazaindacene (BODIPY) derivative as colorimetric and fluorescent probe for cyanide ions, *Org. Lett.*, 2008, **10**, 461–464.
 - 57 R. Luque-Martin, D. C. Angell, M. Kalxdorf, S. Bernard, W. Thompson, H. C. Eberl, C. Ashby, J. Freudenberg, C. Sharp, J. Van den Bossche, W. J. de Jonge, I. Rioja, R. K. Prinjha, A. E. Neele, M. P. J. de Winther and P. K. Mander, IFN- γ drives human monocyte differentiation into highly proinflammatory macrophages that resemble a phenotype relevant to psoriasis, *J. Immunol.*, 2021, **207**, 555–568.



- 58 T. Priem, C. Bouteiller, D. Camporese, X. Brune, J. Hardouin, A. Romieu and P. Y. Renard, A novel sulfonated prosthetic group for [^{18}F]-radiolabelling and imparting water solubility of biomolecules and cyanine fluorophores, *Org. Biomol. Chem.*, 2013, **11**, 469–479.
- 59 G. Vicidomini, P. Bianchini and A. Diaspro, STED super-resolved microscopy, *Nat. Methods*, 2018, **15**, 173–182.
- 60 E. Garcia-Fernandez, S. Pernagallo, J. A. González-Vera, M. J. Ruedas-Rama, J. J. Díaz-Mochón and A. Orte, Time-gated luminescence acquisition for biochemical sensing: miRNA detection, in *Fluorescence in Industry. Springer Series on Fluorescence*, ed. Pedras, B., Springer, 2019, **18**, 213–267.
- 61 L. Wang, B. Chen, W. Yan, Z. Yang, X. Peng, D. Lin, X. Weng, T. Ye and J. Qu, Resolution improvement in STED super-resolution microscopy at low power using a phasor plot approach, *Nanoscale*, 2018, **10**, 16252–16260.
- 62 L. Jiao, C. Yu, J. Wang, E. A. Briggs, N. A. Besley, D. Robinson, M. J. Ruedas-Rama, A. Orte, L. Crovetto, E. M. Talavera, J. M. Alvarez-Pez, M. Van der Auweraer and N. Boens, Unusual spectroscopic and photophysical properties of *meso-tert*-butylBODIPY in comparison to related alkylated BODIPY dyes, *RSC Adv.*, 2015, **5**, 89375–89388.
- 63 J. Catalán, Toward a generalized treatment of the solvent effect based on four empirical scales: dipolarity (SdP, a new scale), polarizability (SP), acidity (SA), and basicity (SB) of the medium, *J. Phys. Chem. B*, 2009, **113**, 5951–5960.
- 64 A. I. Ivanov, in *Exocytosis and Endocytosis*, ed. A. I. Ivanov, Springer New York, New York, NY, 2014, pp. 3–18, DOI: [10.1007/978-1-4939-0944-5_1](https://doi.org/10.1007/978-1-4939-0944-5_1).
- 65 R. D. Klausner, J. G. Donaldson and J. Lippincott-Schwartz, Brefeldin A: insights into the control of membrane traffic and organelle structure, *J. Cell Biol.*, 1992, **116**, 1071–1080.
- 66 E. Macia, M. Ehrlich, R. Massol, E. Boucrot, C. Brunner and T. Kirchhausen, Dynasore, a cell-permeable inhibitor of dynamin, *Dev. Cell*, 2006, **10**, 839–850.

